Eidgenössische Technische Hochschule Zürich
Swiss Federal Institute of Technology Zurich

SED
Schweizerischer Erdbebendienst
Swiss Seismological Service

Report on site characterization

Rothenfluh, Switzerland (ROTHE)

Poggi Valerio, Manel Hobiger, Donat Fäh

Last modified - 24 / 12 / 2014

1. Introduction

In the framework of the NAGRA seismic network project, an array measurement of the ambient vibration wave-field was performed at the location of the SED station ROTHE (Rothenfluh, Switzerland). The scope of the survey is the seismic characterization of the area surrounding the installation (**Figure 1**), which consists in a broadband seismometer (Trillium Compact) with a high-resolution digitizer (Taurus 24Bit @200sps). Ambient vibration analysis has been used to infer the characteristics of the underground structure of the site, with special regard to the one-dimensional shear-wave velocity. Such profile was later used to assess the local seismic response of the station.

For the analysis, different spectral analysis techniques were implemented, consisting in both single and array methods, which are listed below:

- Time-frequency wavelet analysis
- Power-spectral density estimation
- Conventional horizontal to vertical spectral ratios
- Directional horizontal to vertical spectral ratios
- Wavelet polarization analysis
- Three-component high-resolution f-k analysis.

The results of all these analyses conformed to the definition of the final velocity model. In the following, the main results of these investigations are summarized and a final interpretation of the velocity profile is given. From this interpretation, engineering parameters are finally derived, e.g. the Qwl-Vs average velocity, VsZ (including Vs30) and the seismic amplification from the analytical SH-transfer function of the one-dimensional soil column.

2. Survey description

To characterize the seismic response of the site, two array measurements of ambient vibration were performed on 30/01/2014 and on 02/02/2014 (**Figure 1**). Each array consists of a single measuring configuration, of 14 and 11 sensors respectively. The first array (A1) has circular geometry and a diameter of about 120m, while the second (A2), more irregular, has a total aperture of nearly 760m. Performing two separate surveys was imposed by the difficult measuring conditions, mostly related to the dense vegetation of the forest. This dramatically affected the GPS performance for station synchronization and differential localization, which required hours to be completed. In particular, geometry of array A2 was implemented to follow an existing road though the forest. In spite of the dissimilarities in geometry, the two configurations have nevertheless overlapping f-k resolution bands, which assure a continuous mapping of the surface wave phase velocity dispersion curves over frequency. Configuration A1 recorded for a total of 1h00m, while configuration A2 for 2h00m. The differences in the recording length are due to the different resolution characteristics of the two geometries.

As a general rule, larger arrays require longer recording time to produce a reasonable statistics of the ambient vibration processing results. In this case, however, due to an unfortunate presence of strong disturbances induced by human activity (wood log cutting) during acquisition, the usable signal length for configuration A1 was reduced to about 20m only (**Figure 3**). Satisfactory results were nevertheless obtained from the analysis of the two geometries.

High velocities and relatively shallow geophysical bedrock (Hauptrogenstein formation, tabular Jura) were expected for the site. This justifies the use of a large geometry for the array to be successful. However, the maximum aperture of the arrays was again controlled by accessibility through the forest. A precise prior estimation of the possible maximum resolved depth was not possible, due to the large uncertainty of the bedrock velocity and the irregularity of the larger configuration (A2).

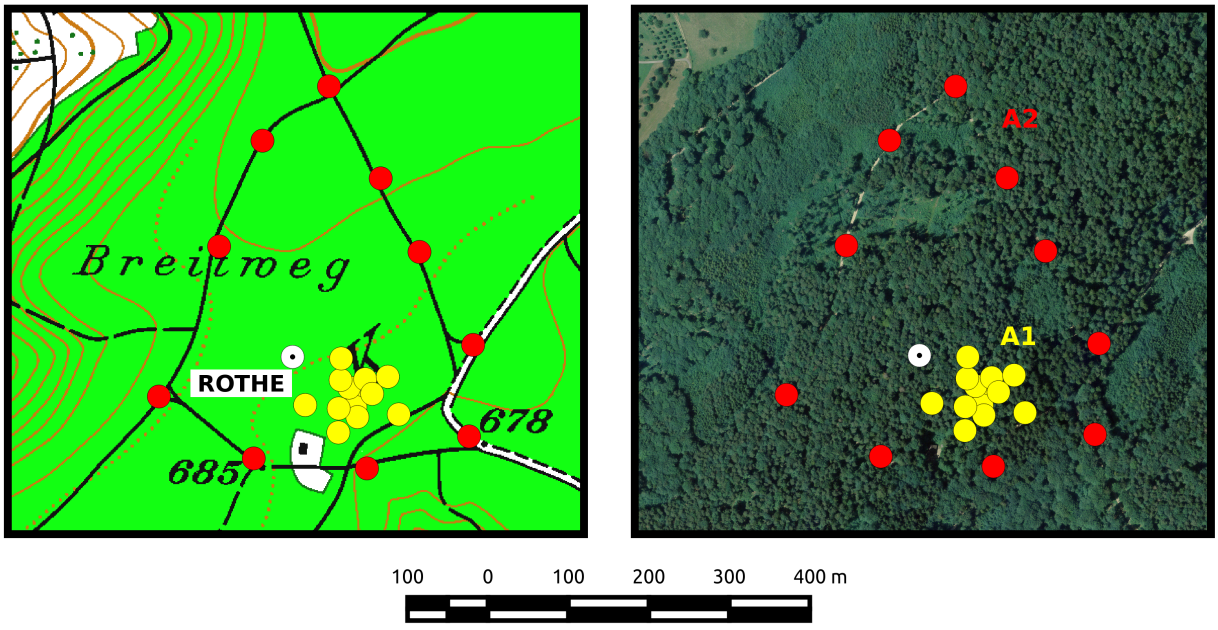

Figure 1 - *Location of the two ambient vibration array surveys performed in Rothenfluh, (SED station ROTHE) on 30/01/2014 and on 02/02/2014. Two concentric configurations of increasing aperture were set up (named A1 in yellow and A2 in red). Location of the permanent station is shown with a white mark.*

3. Soil type, topography and geology

The array has been set in open field conditions, in a protected forest reserve area (**Figure 1**). The influence of buildings and anthropogenic disturbances is virtually negligible, even though some monochromatic harmonic signals affected the second half of the survey (while recording with array configuration A2). Array sensors have been deployed on free soil. Good coupling with the ground was assured by means of digging small holes at the sensor's places, and by using a special support (*Trihedron*®) that facilitates the leveling of the device even for difficult soil conditions. The measurement area was located on top of a small ridge, locally quite flat. However, no topographic correction has been taken into account before processing.

Figure 2 - *Geological map of the region surrounding the measuring area in Rothenfluh (reproduced from Swisstopo, Geologische Generalkarte der Schweiz 1:200000, modified). In red the approximate location of the permanent station ROTHE.*

From the geological points of view (**Figure 2**), the target area is located on a small hill in the South-East portion of the Tabular Jura, within the Hauptrogenstein formation, a marine carbonate formation of Jurassic age (Spatkalk, oolitic limestone). The surface morphology is considerably smooth and modeled by the action of glaciers during the Pleistocene. The calcareous bedrock is likely very shallow at the measuring location, but never exposed across the area (a variable-thick cover of quaternary material is generally present). Such site can be classified as of rock ground-type A.

4. Acquisition equipment

Each acquisition point within the array consisted of a three components seismometer (Lennartz 3C with 5s eigenperiod) and a 24 bit data logger (Quanterra Q330). Synchronization between stations was assured by standard GPS, while a more accurate differential GPS (Leica Viva system) was used to precisely locate the sensor's coordinates with a tolerance of less than 5cm.

5. Weather conditions

The weather conditions were optimal and stable during the whole measurements, with no precipitations, no wind and an average (over the two days) temperature of 7 degrees.

6. Pre-processing and preliminary data-quality control

The three-component recordings have been filtered prior to analysis using a band-pass 6^{th} order causal Butterworth filter with corners at 0.2Hz and 50Hz. Although it is not a strict requirement for spectral analysis techniques, such filtering was applied in order to facilitate the preliminary visual inspection of the noise traces and to evaluate the coherency of the wave-field (**Figure 3**). Such procedure gives essential information for the subsequent interpretation of the f-k analysis results.

By visual inspection of the ambient vibration recordings of array configuration A1, it was evident the presence of about 15m of large amplitude transients, unfortunately induced by the activity of some workers cutting wood logs in the vicinity of the stations. The low quality and not usability of this portion of the signal was later confirmed by preliminary f-k processing. The maximum continuous usable recording length for A1 was then reduced to only 20m (light blue window). The quality was nevertheless sufficient to ensure reliable results. No significant disturbances were apparent on the recordings of array configuration A2.

To assess the quality of the ambient vibration recordings, spectral analysis was subsequently performed. Because of the stochastic nature of the ambient vibration wave-field, a statistical approach has to be used, such as the estimation of the power spectral density (*PSD*). This approach is useful to evaluate the average energy level of the recordings in the analyzed frequency range, and to access the presence of spurious spectral peaks, which might be related to human activity (machinery, pumps). By inspecting the PSD of all the three-component recordings of the array in the range between 0.5 and 40Hz, is found that the average energy level of the spectrum is overall very low, well within the minimum and maximum bounds of the USGS noise model (**Figure 4**). A negligible presence of two harmonic signals of anthropogenic origin is visible on configuration A2 between about 5 and 6Hz. These disturbances however do not affect the quality of the processing.

A) Array 1 - 30/01/2014, 1h00m

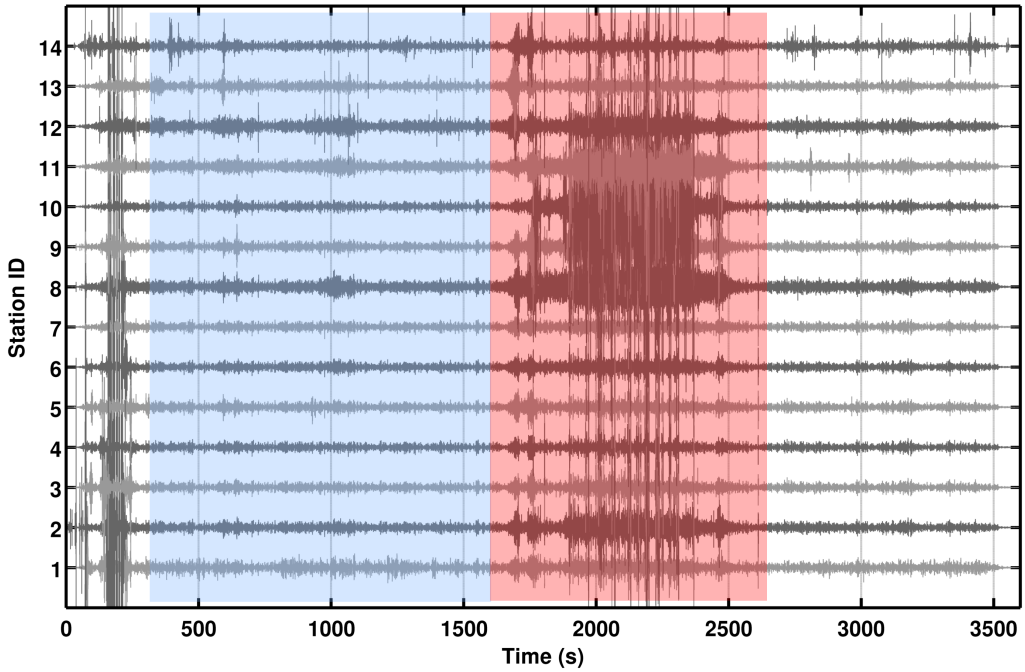

B) Array 2 - 02/02/2014, 2h00m

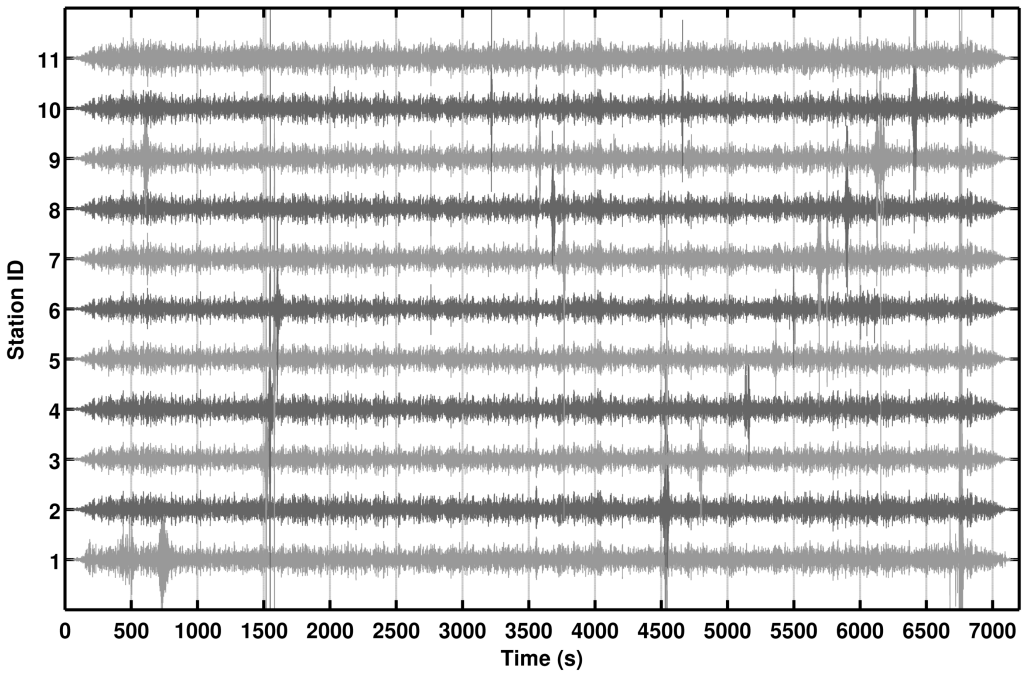

Figure 3 - *Inspection of the quality the ambient vibration recordings of the Rothenfluh arrays (configurations A1 and A2). For array A1, disturbances induced by human activity (red window) limited the usable recording length to about 20m (in light blue).*

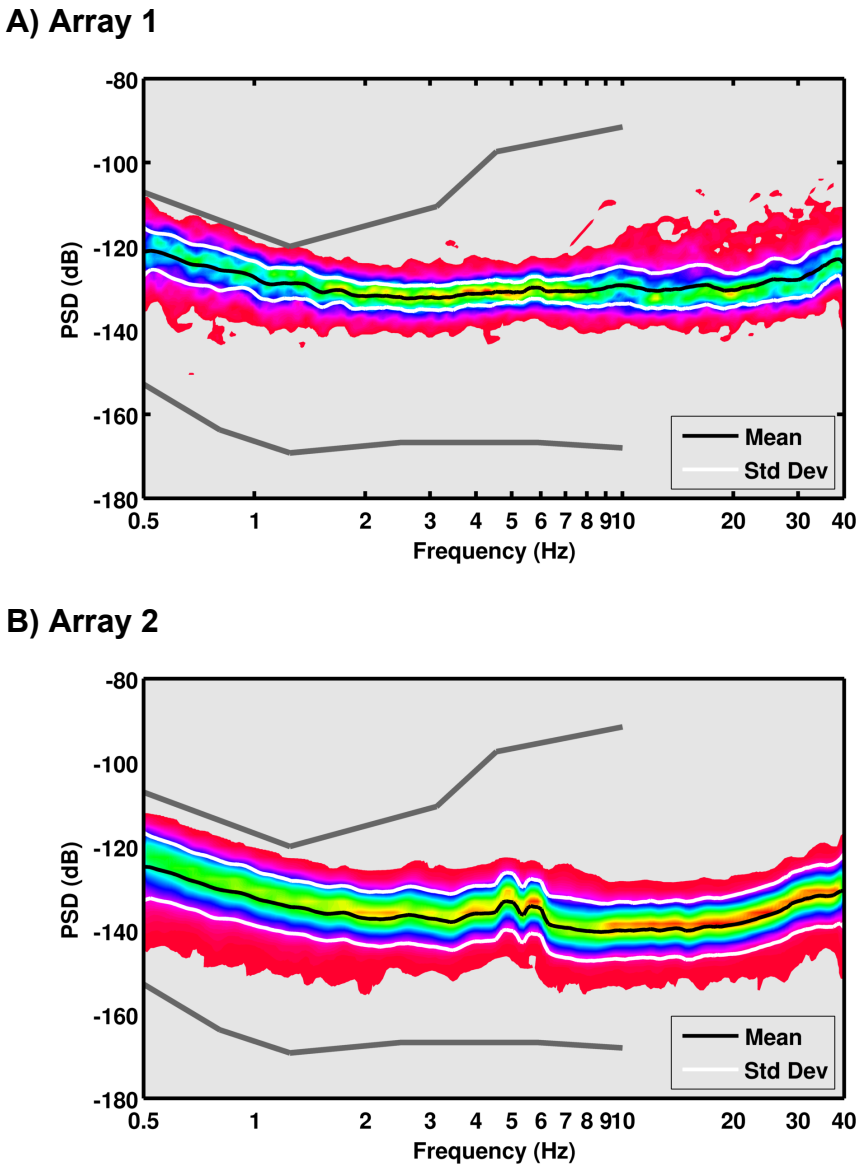

Figure 4 - *Power spectral density (PSD) computed at the central station the array configuration A1 (top) and A2 (bottom), NS component. Similar results were obtained from the other stations and components of the array. In gray lines are the minimum and the maximum bounds of the USGS noise model, for comparison.*

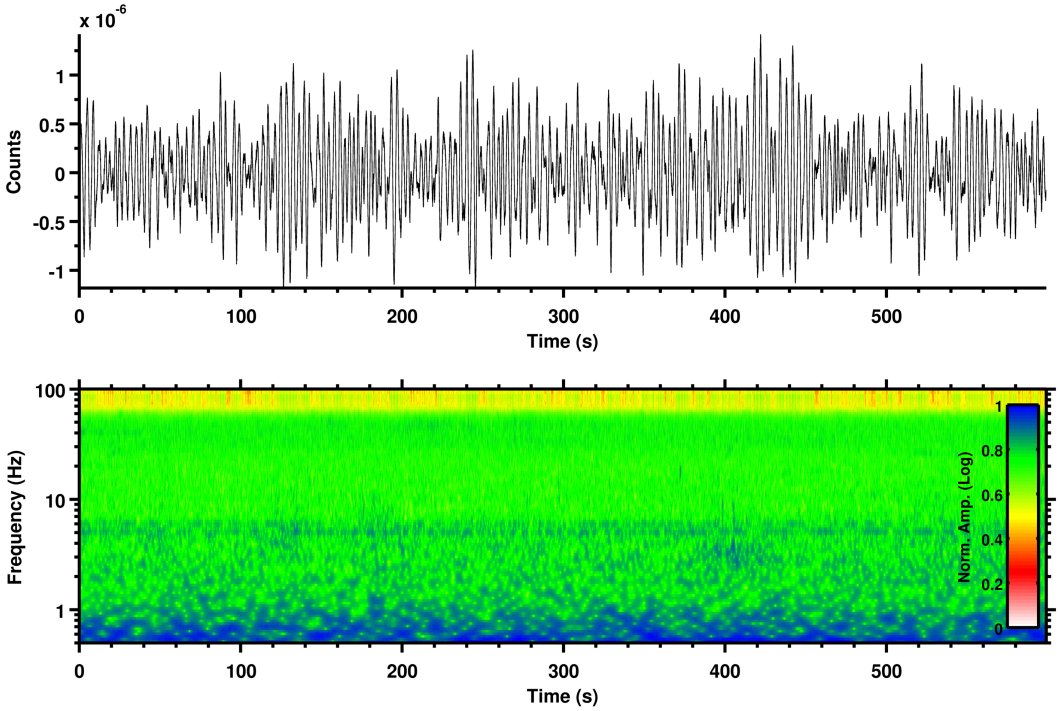

Figure 5 - *Example of spectrogram from 600s of recording of the central station of the array configuration A2. Two negligible harmonic disturbances are visible on the spectrogram, between 5 and 6Hz. These signals were not present during the recordings of configuration A1. For the analysis, the cosine wavelet is used (wavelet parameter = 12).*

Complementary to the aforementioned statistical methods, a spectral decomposition approach is more suitable to assess the stationarity of the ambient vibration wave-field over time. The wavelet time-frequency analysis was then performed over the whole recording time. From such analysis (**Figure 5**) an overall stability of the ambient-vibration wave-field over time is evident. The aforementioned disturbances in A2 at about 5~6Hz are confirmed to be nearly harmonic contributions, more pronounced at the end of the recordings window. This provides a further confirmation of their anthropogenic origin. These disturbances are nevertheless very weak and well localized in frequency; therefore they won't affect the subsequent processing steps.

7. Conventional H/V spectral ratios

The horizontal-to-vertical (H/V) Fourier spectral ratio is a technique widely used in seismic site characterization because of its ability to provide an estimate of the SH wave fundamental frequency of resonance (f_0) of the site. Other than that, H/V ratios are useful to provide information on the Rayleigh wave ellipticity function, which can be used in surface wave dispersion inversion procedures to constrain large velocity contrasts at depth. In this study, we use the H/V technique also to map the variability of the subsoil structure along the investigated area; this is necessary to verify the fulfillment of the 1D structure assumption, which is necessary for the f-k method applied later.

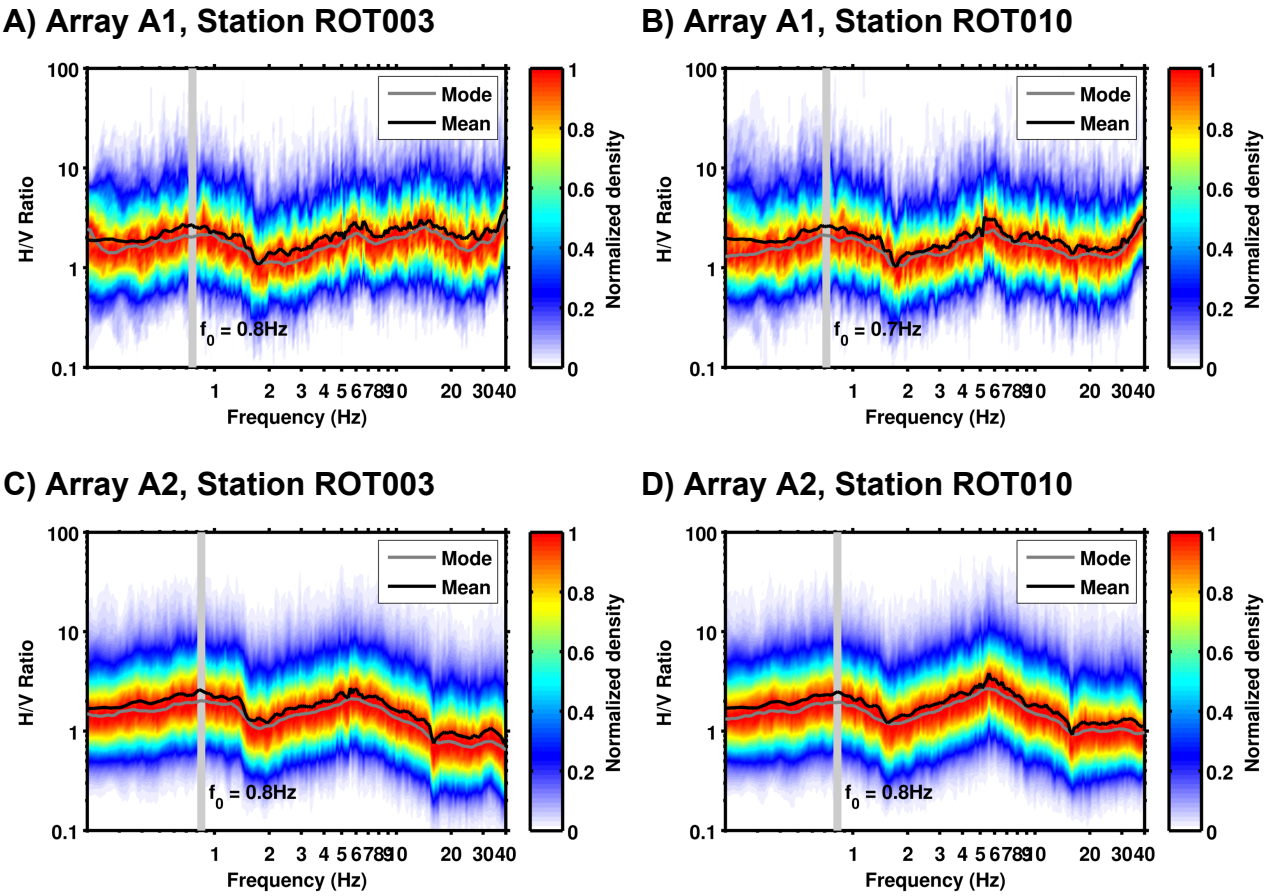

Figure 6 - *Example of H/V spectral ratios for the two concentric configurations A1 and A2. With the exception of the very high frequency range, H/V curves are stable on all stations and between array geometries. The resonance frequency is indicated with a light gray line. An additional peak is also present at about 6Hz, but with more variability.*

H/V spectral ratios have been computed for all the recordings at each station of the array and separately for configurations A1 and A2 (e.g. **Figure 6**). H/V curves have relatively low amplitudes and their shape is compatible with typical of stiff-soil/rock velocity profiles. The behavior of the noise wave-field at the different stations location is very comparable (**Figure 7**). A relatively small peak is always visible at low frequency (around 0.7~0.8Hz), quite stable over the whole measuring area. Such maximum is likely induced by a change in lithology at large depth, which causes a moderate contrast of seismic impedance. The peak should be regarded as the fundamental resonance frequency of the site. A second peak at about 6Hz is also present, with slightly larger amplitude (between 2 and 3). This second peak is of more difficult interpretation, as it could be addressable to a further velocity contrast or to a secondary maximum in the Rayleigh wave ellipticity function. This aspect will be clarified later in the analysis. Finally, the high frequency region (> 8~10Hz) is more variable within and between the two array configurations. In this range, H/V curves are however more diverse in A1 than A2. This can be explained by the difference in soil cover between the geometries, which was unconsolidated detritus in A1, and compacted ground in A2 (along the road).

8. Directional analysis

The computation of directional H/V spectral ratio or polarization analysis is useful to reveal asymmetries in the ambient vibration wave-field. Different effects can induce such a behavior: 2D/3D structure, topographic effects or a non-homogeneous distribution of the noise sources. If a strong directionality is found by the analysis, it is generally recommended to carry out further investigations to properly address the origin of polarization.

By processing the directional H/V ratios at all the recording stations of the two arrays (e.g. **Figure 8**) it is possible to observe an overall isotropy of the wave-field in the low to intermediate frequency range, roughly below 6Hz. The fundamental frequency peak at about 0.8Hz does not show any preferential directionality pattern between the different station locations. Conversely, the secondary peak reveals in several stations of the array A2 a moderate directionality towards E-W. Such behavior is also present - but nevertheless far less evident - in some stations of array A1.

The results of the H/V directional analysis are partially confirmed by applying the wavelet polarization analysis techniques as described in Burjanek et al. (2008). Also in this case no sign of significant directionality (**Figure 9**A) and polarization (**Figure 9**B) of the wave-field is observable in the low frequency band. Here, however, no preferential polarization direction is observed for the secondary maximum.

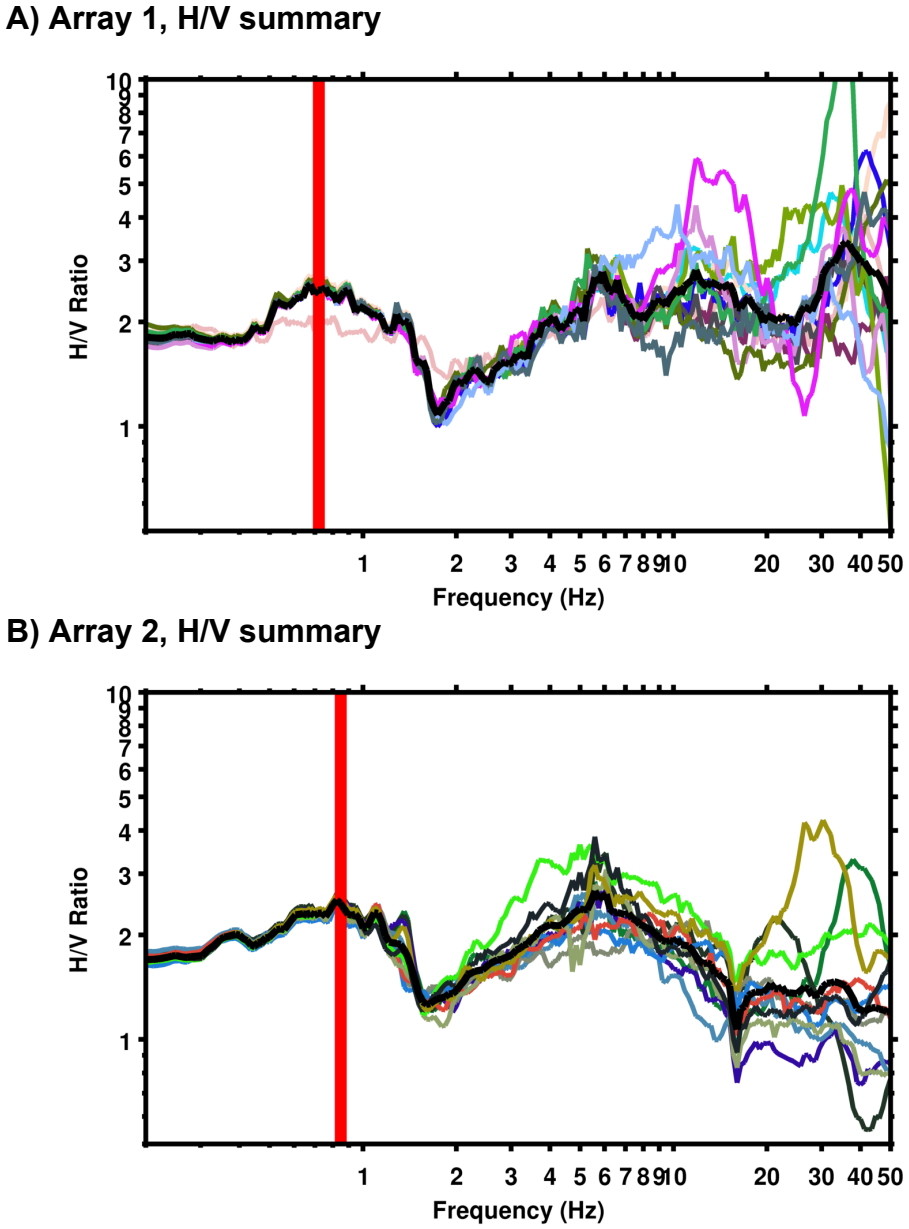

Figure 7 - *Comparison of H/V spectral ratio curves for all the stations of the array A1 and A2. The fundamental frequency can be identified at about 0.7~0.8Hz. The curves are stable and comparable up to the secondary maximum at about 6Hz, confirming the lateral homogeneity of the underlying deep velocity structure of the site. At high frequencies spectral ratios are more variable across the arrays. This reflects the heterogeneity of the soil cover.*

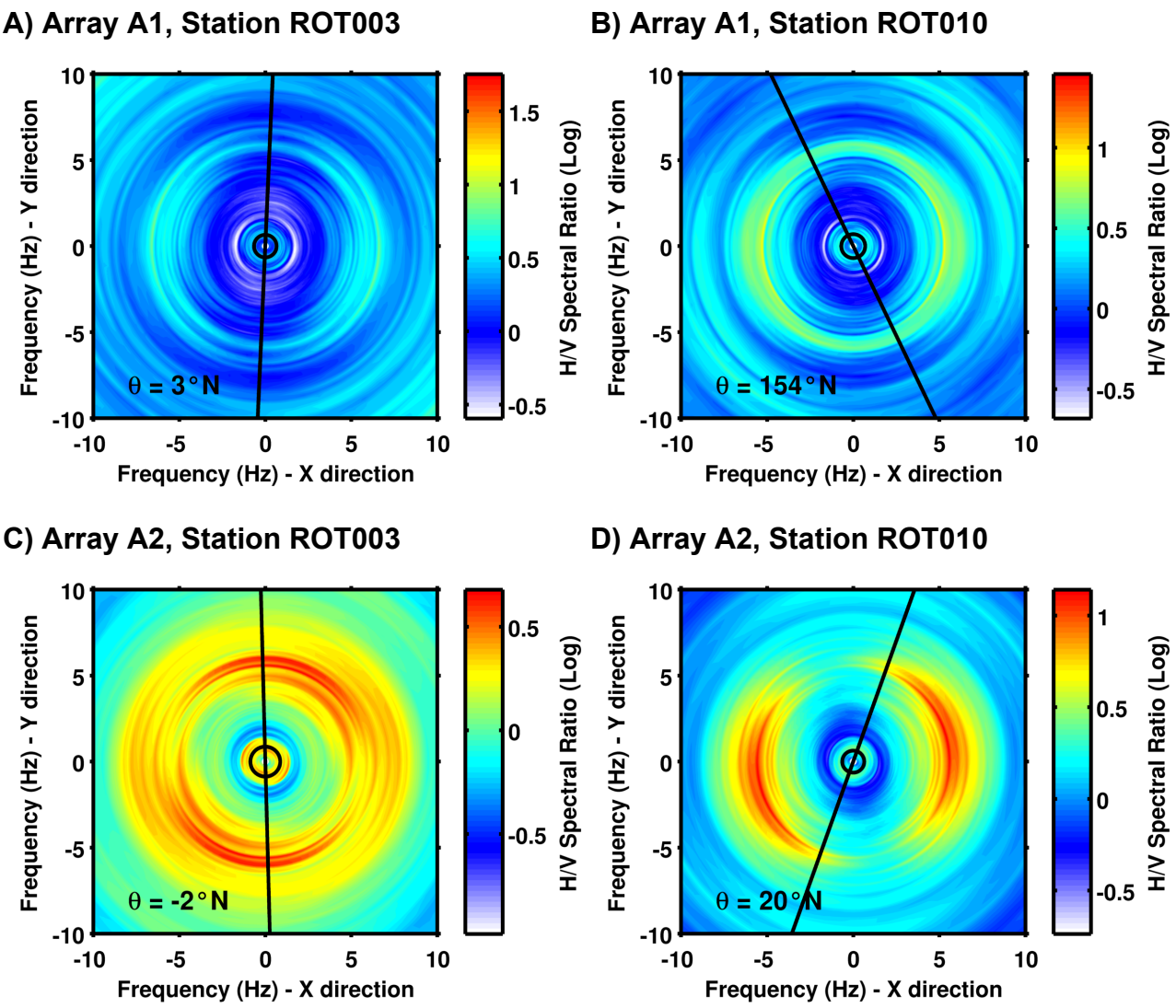

Figure 8 - *Example of directional H/V spectral ratios for the two array configurations A1 and A2. No evidence of wave-field anisotropy is present in the low frequency range (up to about 6Hz), while the secondary H/V peak is preferentially aligned toward E-W in many stations of array configuration A2. This behavior is nevertheless less evident within the stations of configuration A1.*

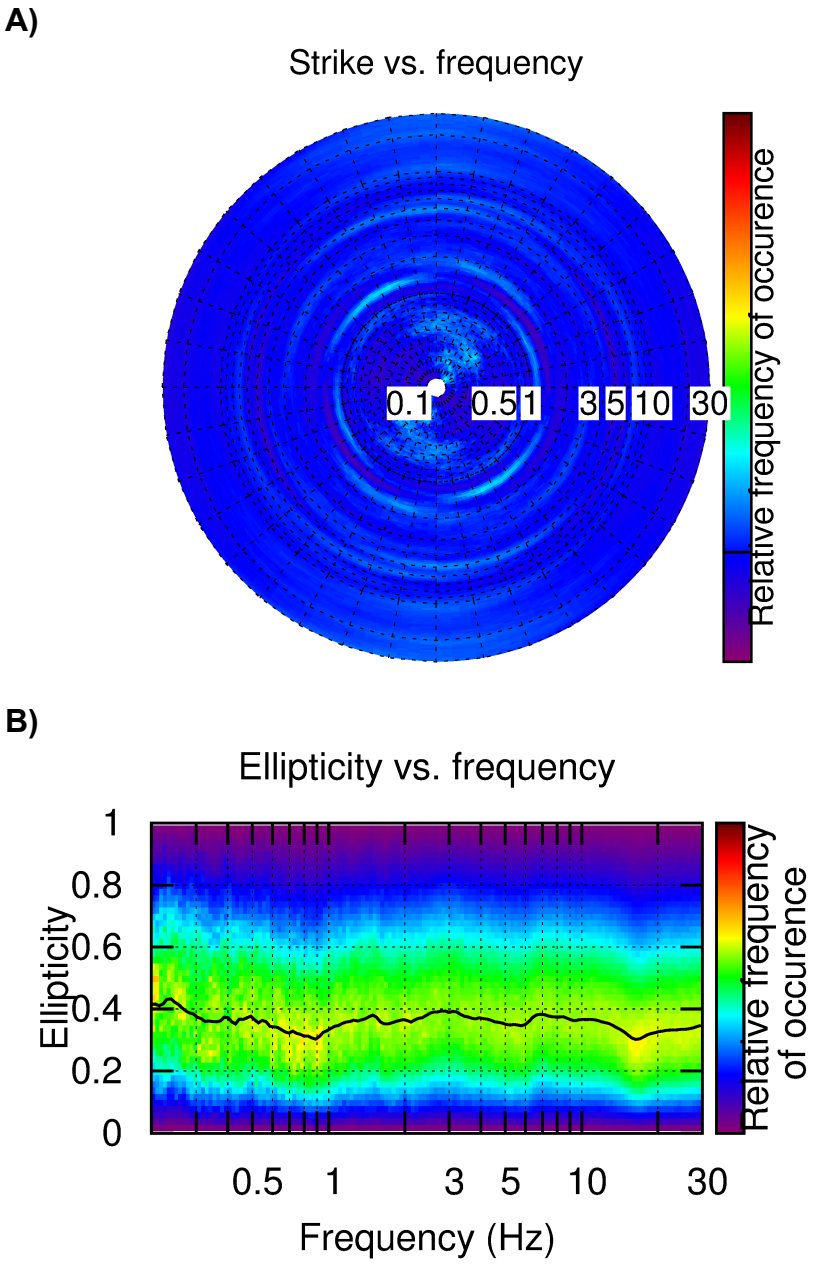

Figure 9 – *Example of wavelet-based polarization analysis at the station ROT003 of the array configuration A1. By analyzing the polarization over strike (A) and the particle motion ellipticity plot (B), no directional effect is visible in the frequency range of interest.*

9. Three-component f-k analysis

The frequency-wavenumber analysis is a spectral technique based on seismic array recordings that allows retrieving direction and dispersion characteristics of the surface waves. We apply this technique to three-component ambient vibration recordings using a modification of the high-resolution method of Capon (1969) as described in Poggi et al. (2010). Using all the three-components of motion gives the possibility to retrieve information about the propagation of the Rayleigh waves (vertical and radial processing direction) as well as of the Love waves (transversal direction).

As in the case of the previous methods, the ambient vibration recordings are treated statistically by subdividing the traces in sub-windows. For each consecutive window a separated f-k analysis is performed, and the results are then averaged over the whole recording, increasing the robustness of the final estimation.

A) 2-4Hz

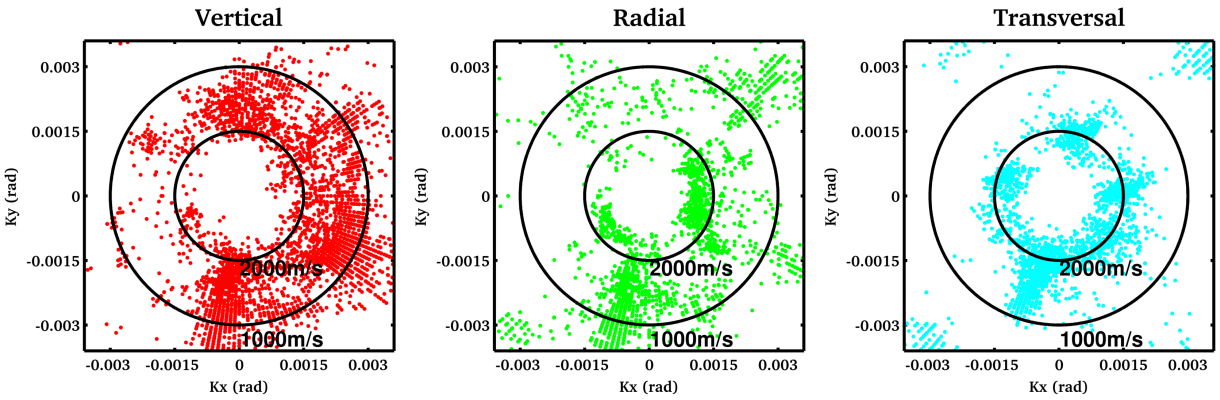

B) 4-8Hz

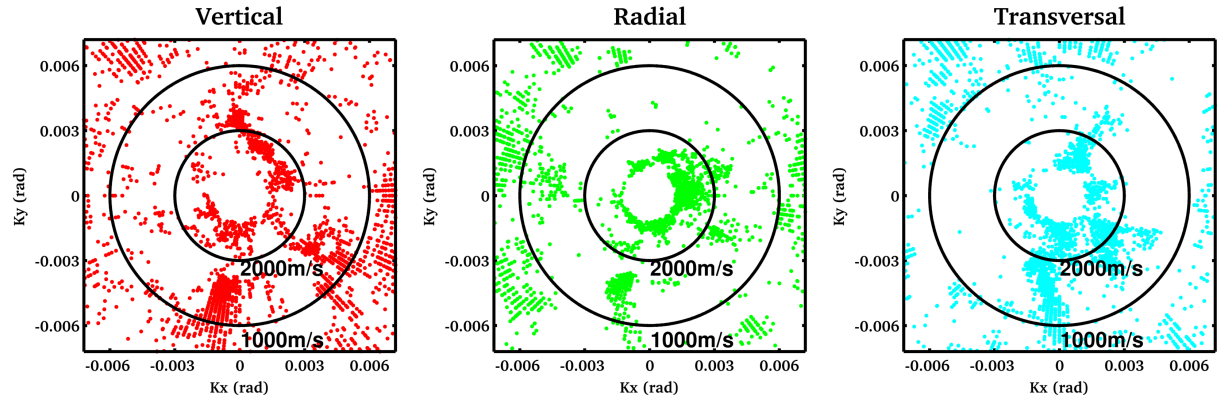

Figure 10 - *Example of distribution of noise sources in the low (2-4Hz) and intermediate frequency range (4-8Hz) obtained from three-component f-k analysis of A2. The source distribution is irregular but not strictly directional on all the propagation components.*

As first step, from the f-k analysis it is possible to assess the noise source azimuthal distribution for different frequency ranges (e.g. **Figure 10**) separately for the vertical, the radial and the transversal direction of polarization. From the analysis of the two geometries A1 and A2, source distribution appears to be quite inhomogeneous in all the components, without nevertheless displaying a clear directional pattern.

As a second step, the surface-wave dispersion curves are extracted by visual inspection and manual picking of the f-k density plots (**Figure 11** and **Figure 12**), separately for the three polarization direction. Complementary results have been obtained for the two array configurations A1 and A2, whose resolution limits partially overlap.

Rayleigh wave dispersion can be well tracked for A1 on both the vertical and the radial components (**Figure 11**). Here, a single mode with nearly constant velocity can be well identified on a broad frequency range. Only at very high frequency the mode seems to be bending to lower velocities (of doubtful interpretation, given the frequency). Results from A1 are complemented at low frequencies by the f-k processing of A2 (**Figure 12**), which extends the resolution on the mode down to about 1.6Hz. As well, Love wave dispersion is also resolved in array configuration 1, but nearly invisible in the processing from configuration 2. The results from the two arrays are also not perfectly matching in velocity. A summary of all the preliminary identified modes from vertical, radial and transversal direction of propagation is presented in **Figure 13**.

For the modal interpretation we proposed two alternative models. In the first model we assume the Rayleigh and Love dispersion described by a single fundamental mode (**Figure 14**A). Such pattern is common in rock sites without strong variations of velocity with depth. Alternatively, for the second model we propose a more complex interpretation, based on the possibility of existence of several consecutive higher modes close to osculation (**Figure 14**B). In such a case, the modal energy may transfer from a mode to the subsequent, giving rise to an observed modal pattern with apparent nearly-constant phase velocity (similar cases are well documented in literature related to active surface wave analysis). According to this hypothesis, the identified Rayleigh mode is then split into three independent modes (one fundamental and two higher) at those frequencies where the dispersion curve shows large irregularities (~5Hz and ~10Hz). Same approach is therefore applied to Love dispersion too, as a single mode was found not compatible with multimodal Rayleigh dispersion (as we later tested).

10. Inversion of the dispersion curves

The surface wave dispersion curves (Rayleigh and Love) obtained from the three-component f-k analysis of the ambient vibrations are inverted to obtain an estimation of the velocity profile of the site (mainly S-wave velocity as function of depth, and to a lesser extend the P-wave velocity, due to the lower sensitivity). The analysis is performed using the software *Dinver* (www.geopsy.org), which implements a direct search approach (e.g. **Figure 15** and **Figure 16**) based on a conditional version of the neighborhood algorithm (Sambridge, 1999).

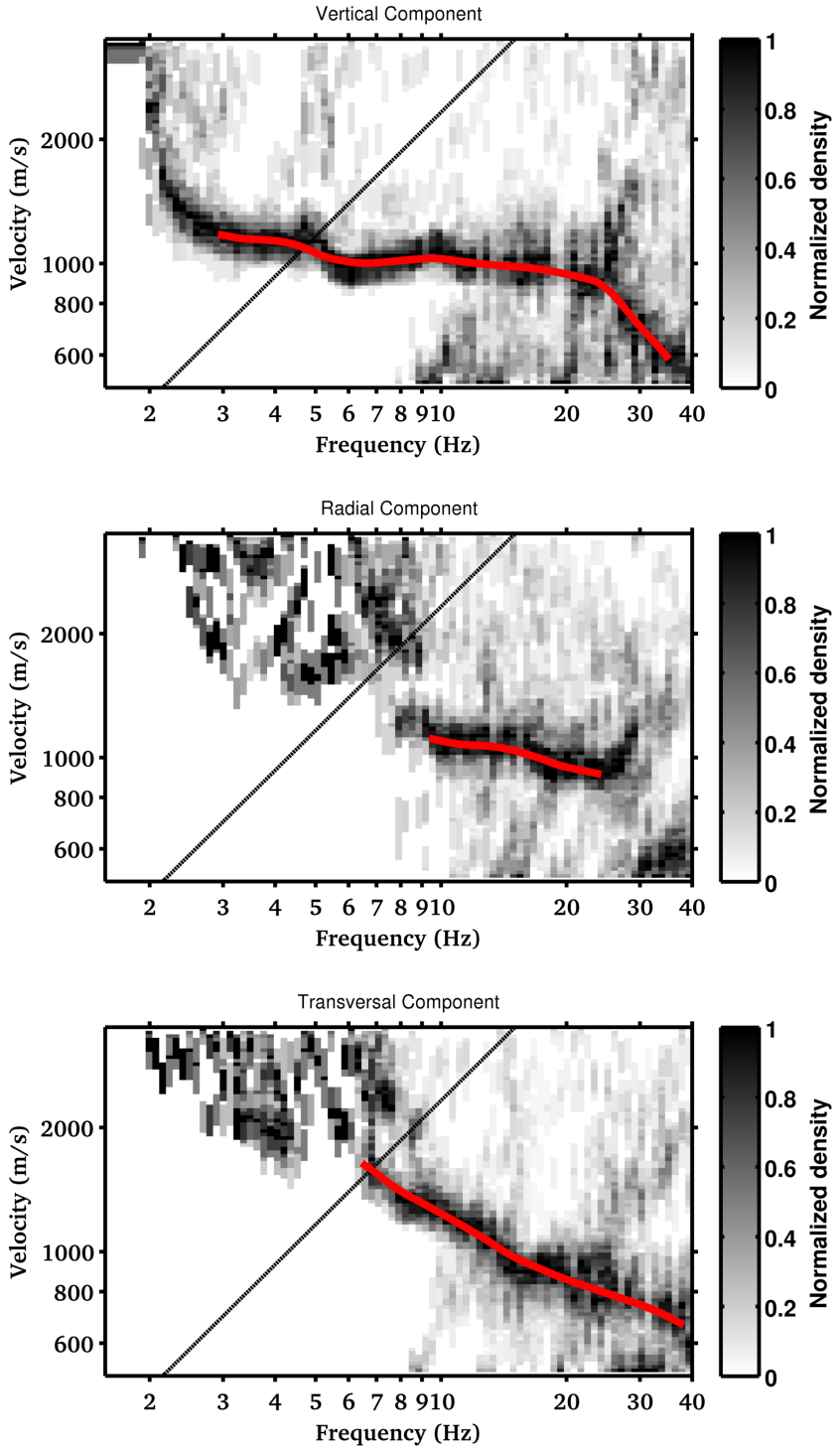

Figure 11 - *Density distribution of the surface wave signals obtained from the recording of the array configuration A1 using three-component f-k analysis. From top to bottom: Rayleigh vertical, Rayleigh radial and Love wave dispersion. In red the preliminary interpreted dispersion curves are given (manually selected).*

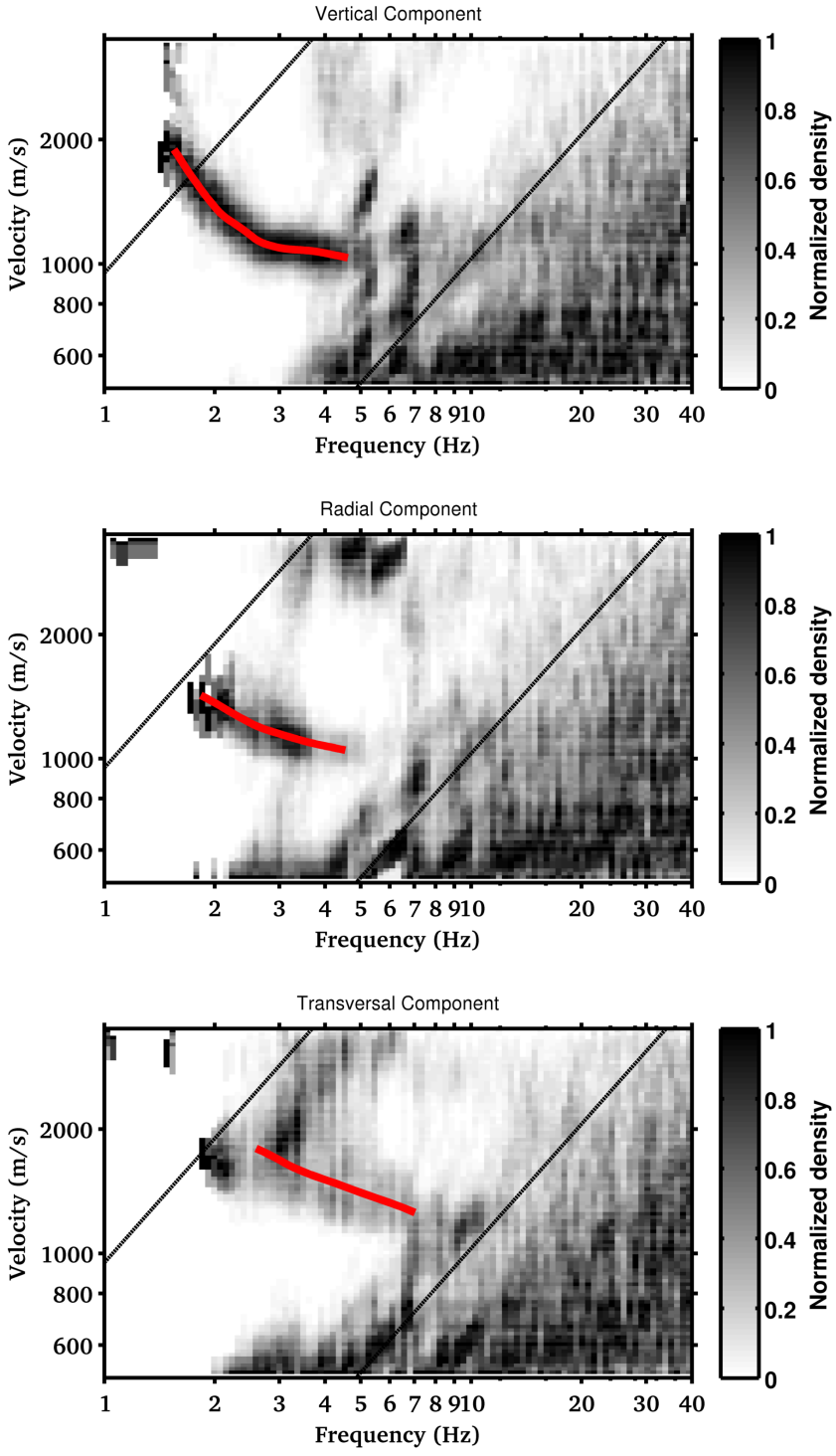

Figure 12 - *Density distribution of the surface wave signals obtained from the recording of the array configuration A2 using three-component f-k analysis. From top to bottom: Rayleigh vertical, Rayleigh radial and Love wave dispersion. In red the preliminary interpreted dispersion curves are given (manually selected).*

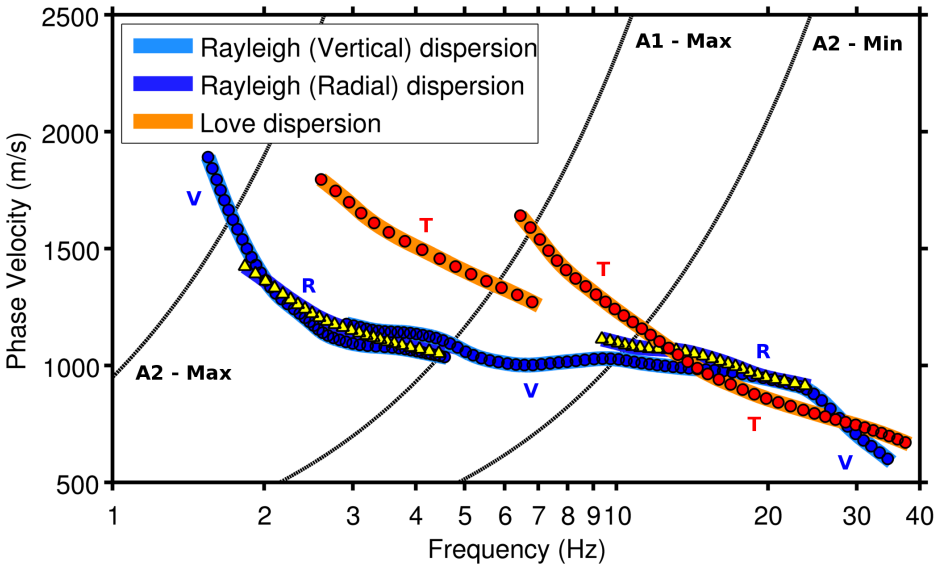

Figure 13 - *Summary of all picked dispersion curves obtained from three-component f-k analysis of the two array configurations A1 and A2. Minimum and maximum resolution bounds of the two array geometries are indicated with black solid lines.*

To parameterize the velocity model, two different approaches were implemented. The first one consisted in setting up an eight-layer model with fix interface depths (**Figure 17** A and C). In such a case the free inversion parameters are then the velocities (P and S) and layer thicknesses. In the second case, a free-thickness layer approach was used (**Figure 17** B and D). The advantage of the former method stays in the possibility to better resolve sharp velocity interfaces, while the second is less unique and better constraints the seismic velocity. The two approaches have to be nevertheless considered complementary, and they should provide consistent results. Ten inversion tests (*runs*) were performed for each of the two interpretation schemes (single mode and multimode), in order to minimize the effect related to a possible unfavorable initial randomization of the parameter space. The best fitting model from of each run was then collected, evaluated and used for the computation of the derived soil parameters.

A) Single mode model

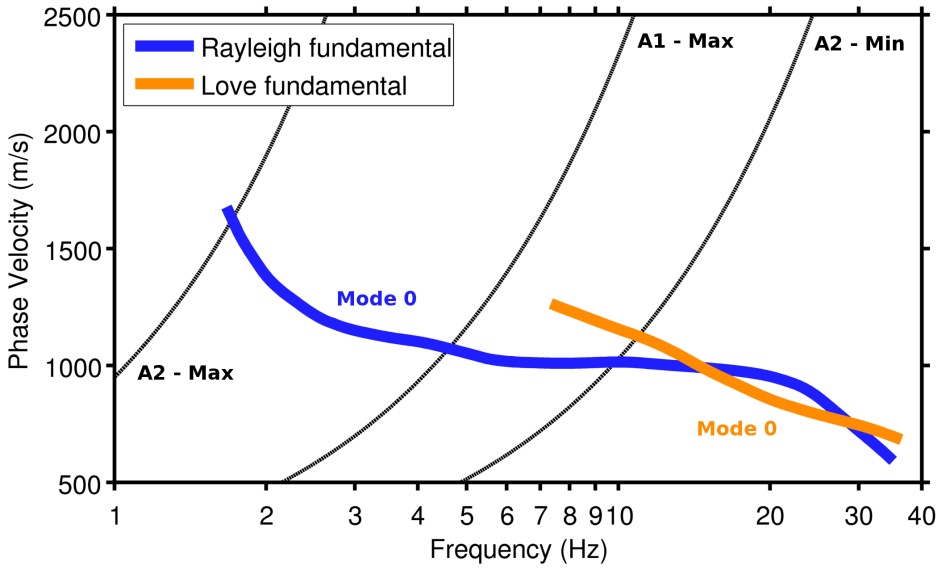

B) Multimode model

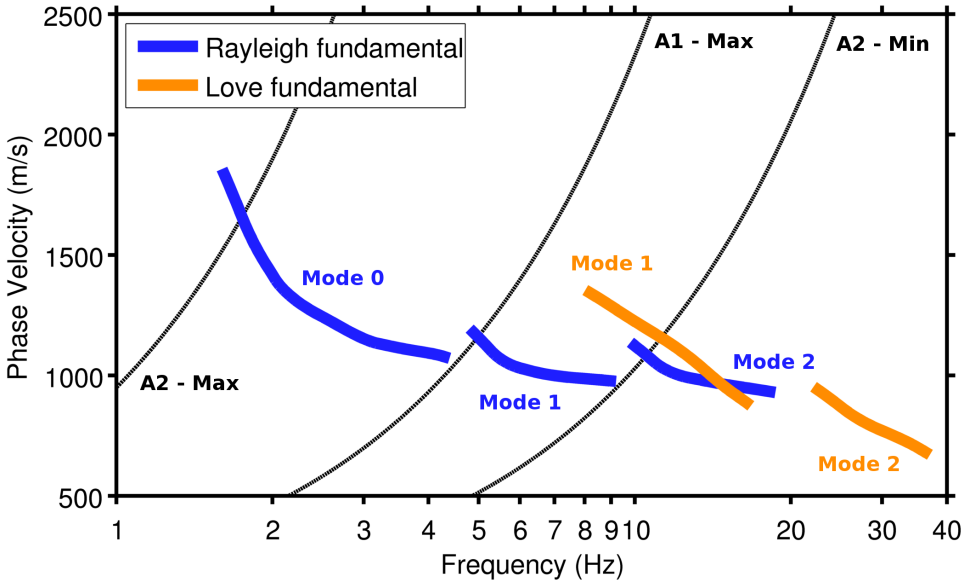

Figure 14 - *Final interpretation of the Rayleigh and Love dispersion curves for ROTHE. Two independent models are presented for comparison (named "single mode" and "multimode"). Minimum and maximum resolution bounds of the two array geometries are indicated with black solid lines.*

A) Single mode model, Love waves

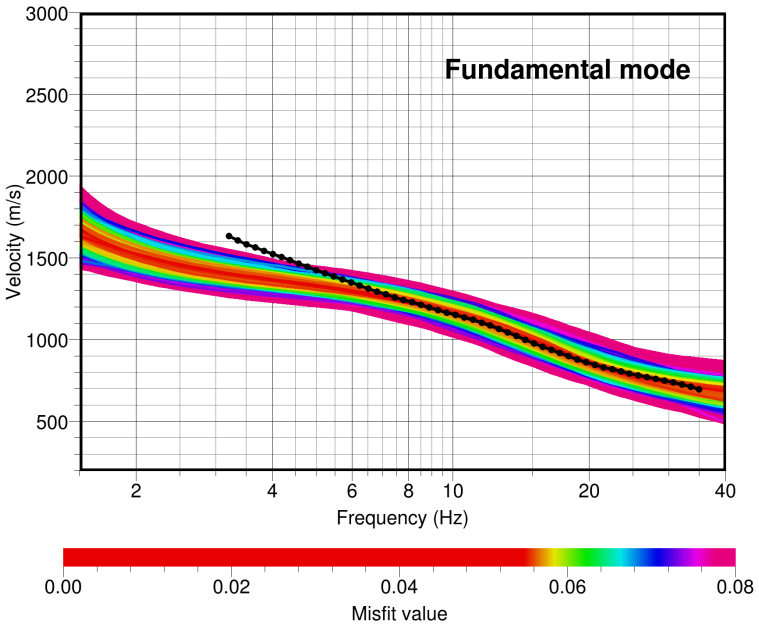

B) Single mode model, Rayleigh waves

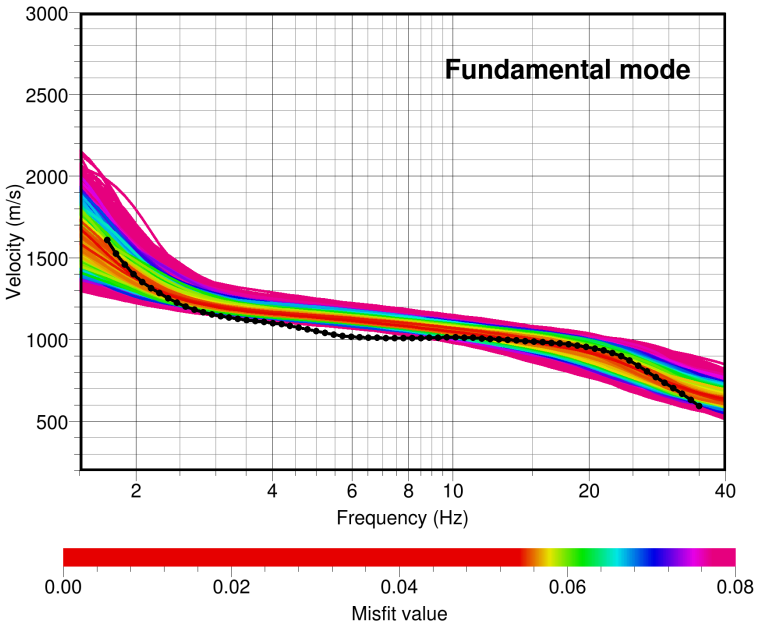

Figure 15 - *Fitting of the surface dispersion data within the global optimization inversion of the "single mode" interpretation. Different colors represent different misfit between the observed (in black) and the modeled dispersion curves during the search.*

A) Multimode model, Love waves

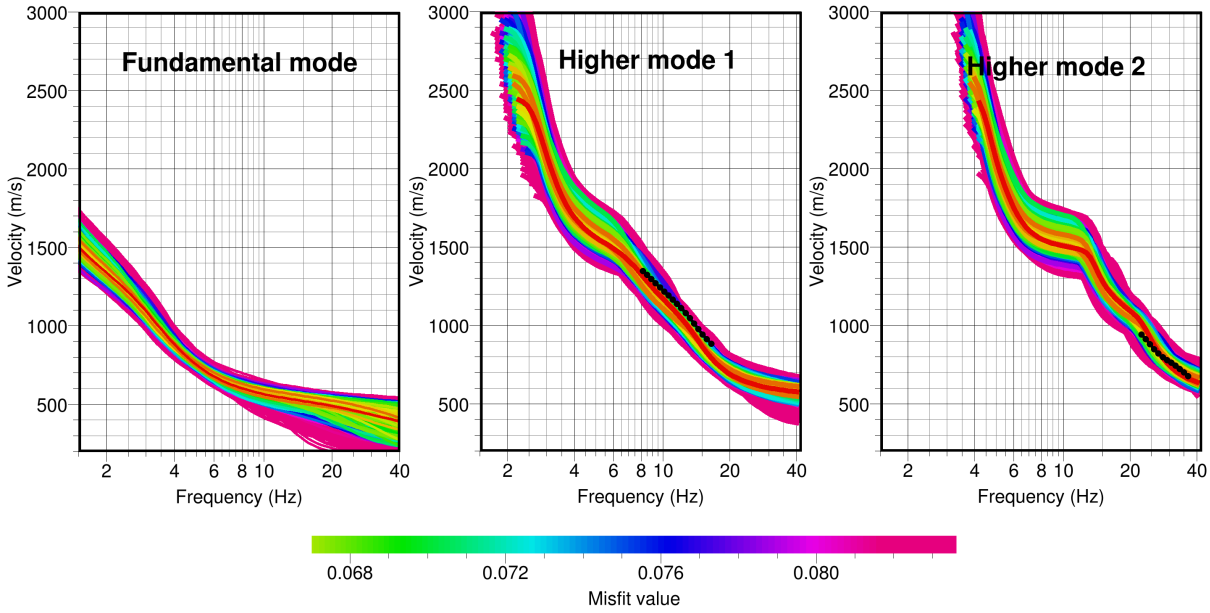

B) Multimode model, Rayleigh waves

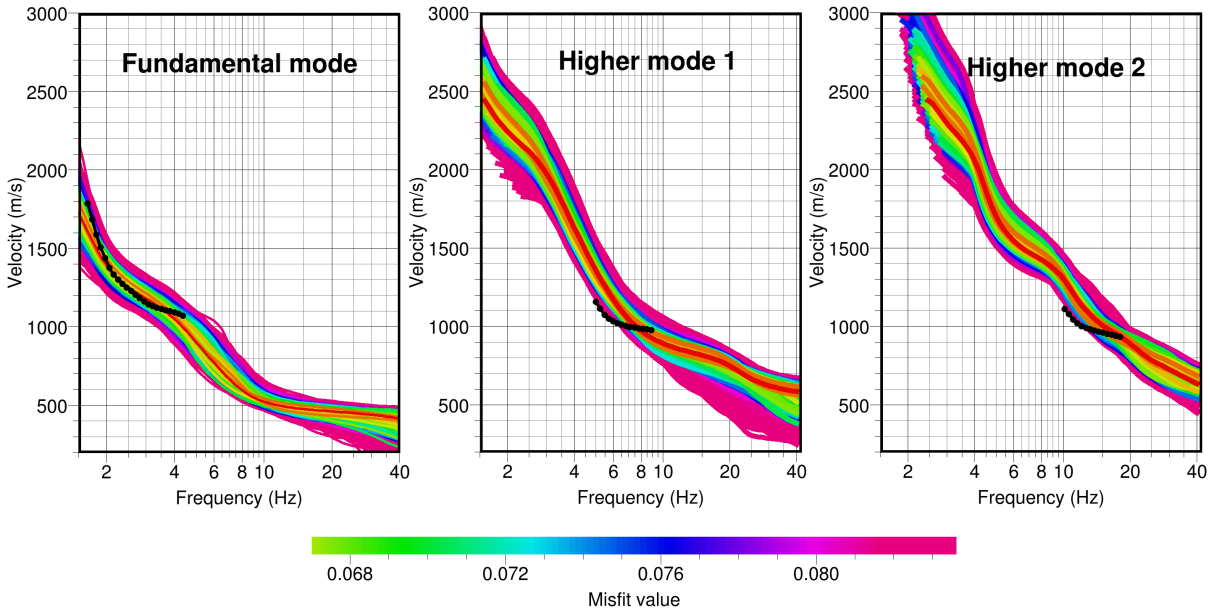

Figure 16 - *Fitting of the surface dispersion data within the global optimization inversion of the "multimode" interpretation. Different colors represent different misfit between the observed (in black) and the modeled dispersion curves during the search.*

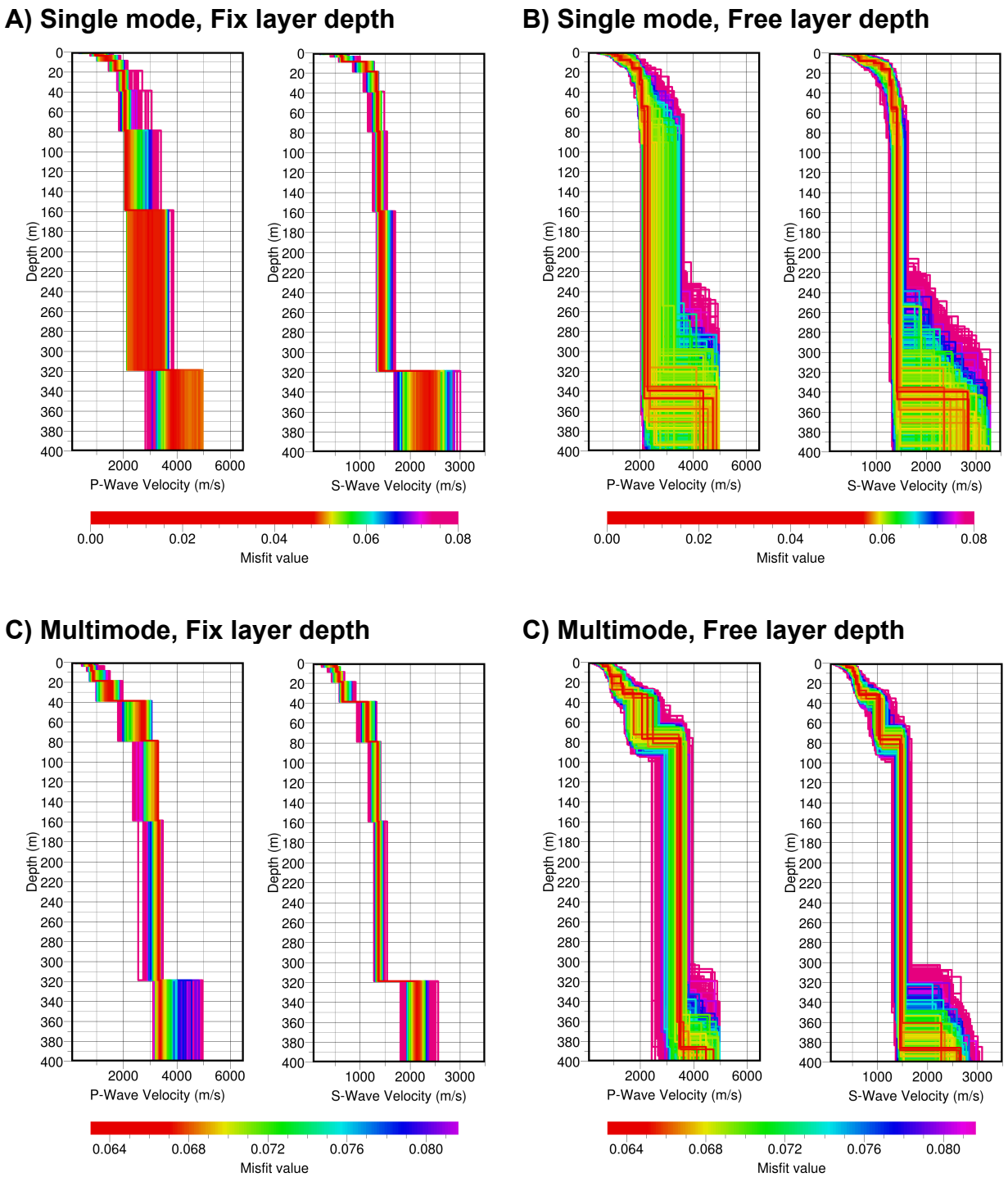

Figure 17 - *Distribution of the free- and fix-layer velocity models generated during the inversion process, ordered by decreasing misfit, according to the color scheme of* **Figure 15** *and* **Figure 16**.

A) Single Mode model **B) Multimode model**

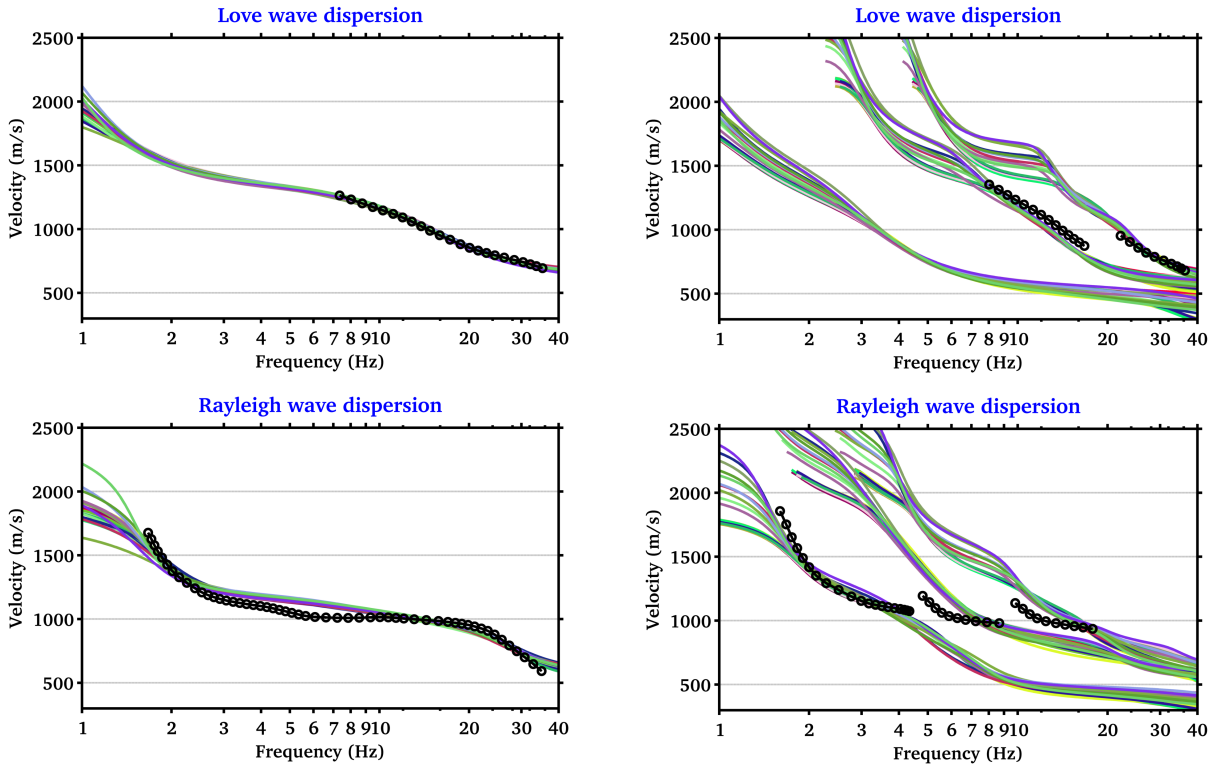

Figure 18 - *Dispersion curves computed from the best fitting models of the two proposed interpretation schemes; pictures include all inversion runs performed using both the free-layers and fixed-layers parameterization schemes.*

In more detail, the inverted velocity models (Vs and Vp) for the two proposed interpretations are quite dissimilar, particularly in the shallower part of the profile. Results from "single mode" interpretation are gradient-like, with a faster increase in velocity in the first 20m, followed by a smoother and nearly-constant velocity part. This is realistically expected for a rock site. Results from "multimode" model have a more complex structure, with two evident velocity jumps at about 25m and 80m and of relatively high impedance contrast. At larger depth, S-wave velocities are comparable for both the schemes, while Vp is considerably different. The deeper interface at about 350~450m is solely constrained by inverting the Rayleigh wave ellipticity peak obtained from H/V analysis. Below this value no direct constrain is available from f-k analysis, and the velocity values are defined by pure extrapolation.

A) Single Mode model

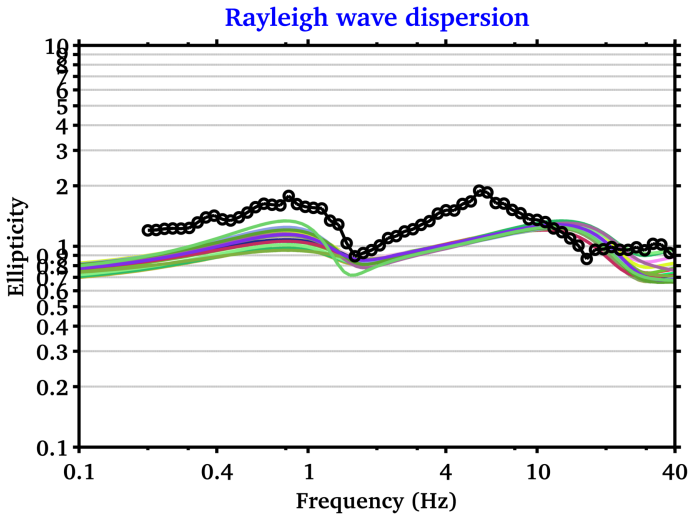

B) Multimode model

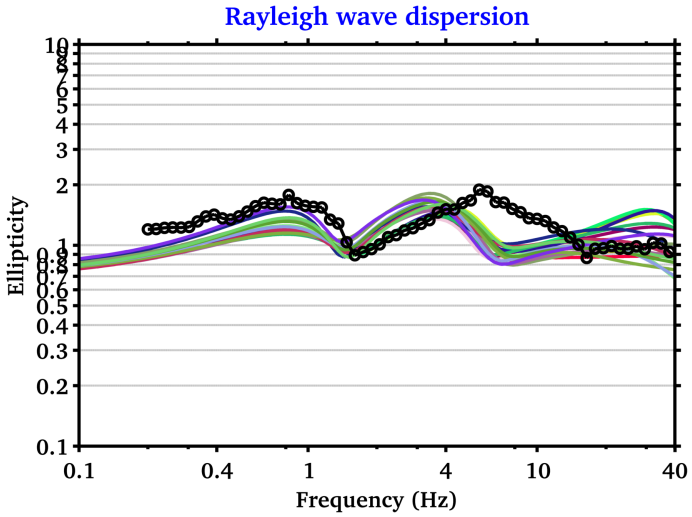

Figure 19 – *Rayleigh ellipticity curves computed from the best fitting models of the two proposed interpretation schemes; pictures include all inversion runs performed using both the free-layers and fixed-layers parameterization schemes. Only the first ellipticity peak was used as constraint for the inversion.*

A) Single mode model

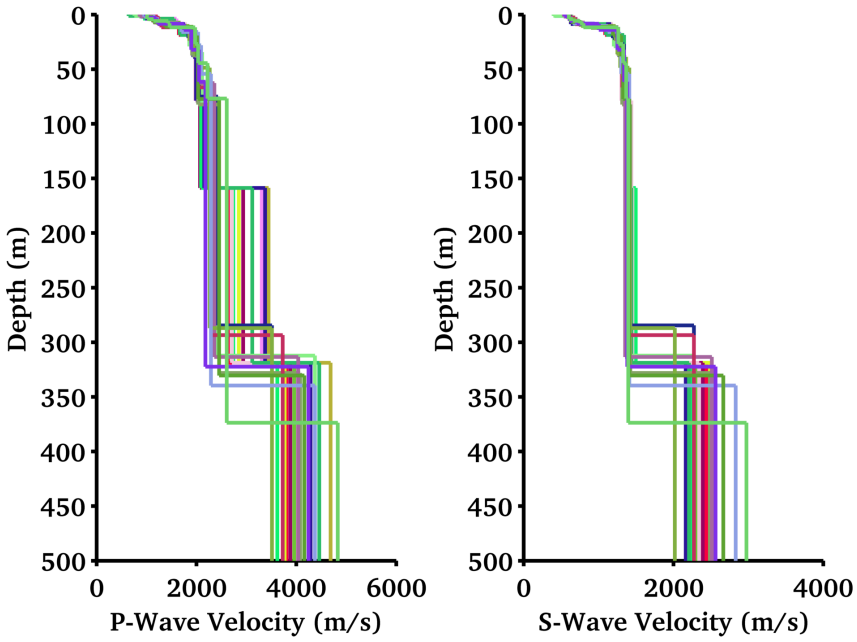

B) Multimode model

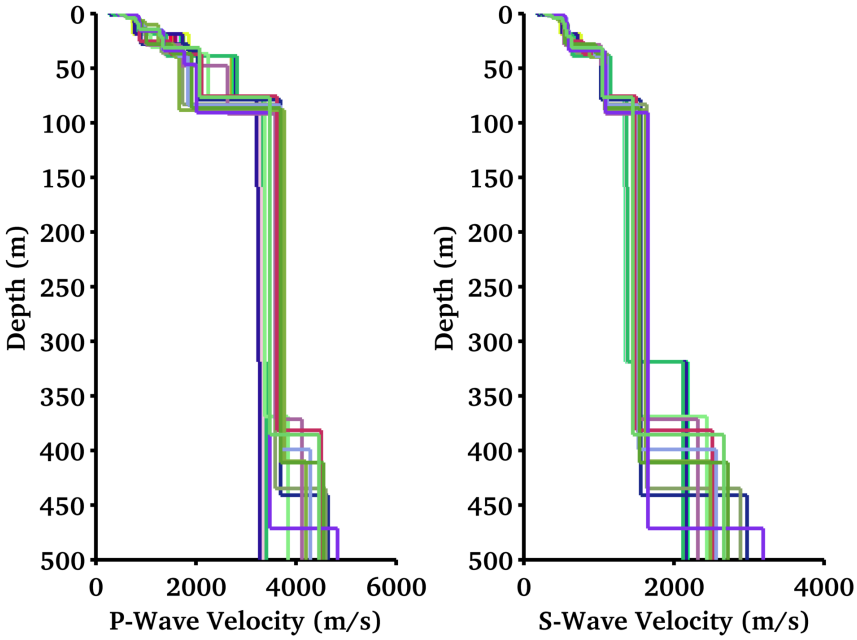

Figure 20 - *Best fitting models of the two proposed interpretation schemes; pictures include all inversion runs performed using both the free-layers and fixed-layers parameterization schemes.*

11. Amplification models

Synthetic site amplification is computed using two different approaches: the S-wave transfer function for vertical propagation and the quarter-wavelength approach. In general the first method is used to evaluate the resonance characteristics of the site, while the second is more useful to assess the effect of the velocity contrasts between the lowermost rock layer (as reference) and the different QWL averaging depths. The two amplification functions are then corrected for the Swiss rock reference velocity profile as defined in Poggi et al. (2011), according to the procedure described in Edwards et al. (2013). Given the lower velocities in the uppermost part of the ROTHE profile compared to the Swiss reference, the final corrected amplification function shows a lower average amplification level at high frequencies than the uncorrected (e.g. **Figure 21**). It has to be notice that the amplification functions do not include attenuation at this stage of the analysis, as the quality factors of the site are unknown.

Amplification computed from the two sets of inverted models (**Figure 22**) is then compared with empirical amplification from spectral modeling of low magnate events (Edwards and Fäh, 2013). Results obtained from the "single mode" models show to be more consistent with observations than those from the "multimode" approach. This last, in more detail, shows higher amplification in the intermediate frequency range (2-10Hz) not supported by data. Such amplification is related to the impedance contrasts at 25m and 80m. For this reason, the "single mode" model is finally selected as representative for the site.

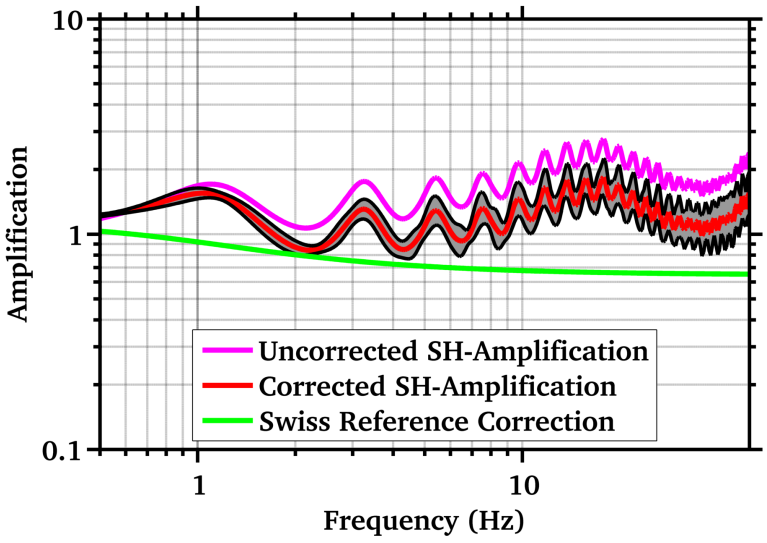

Figure 21 - *Example of correcting the SH-wave transfer function for the Swiss (rock) reference conditions (Poggi et al. 2011). The final corrected amplification function shows a lower (average) amplification at high frequencies than the uncorrected. In this example, amplification is computed from the single mode inversion model.*

A) Single mode model

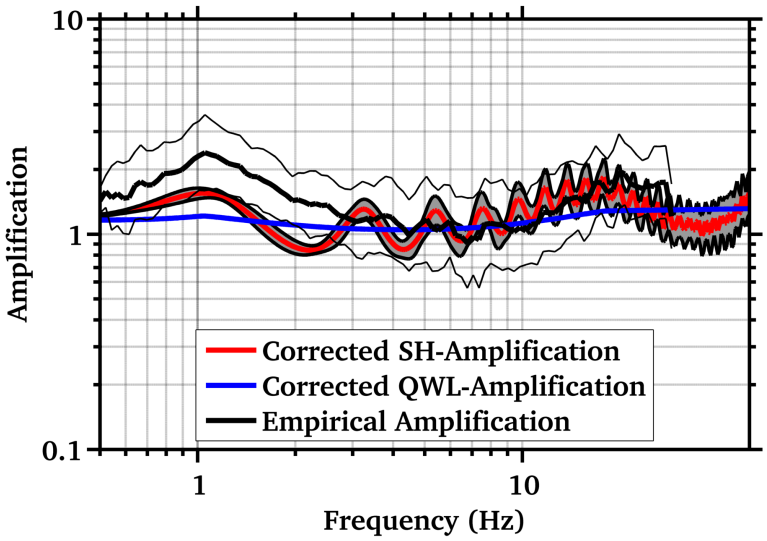

B) Multimode model

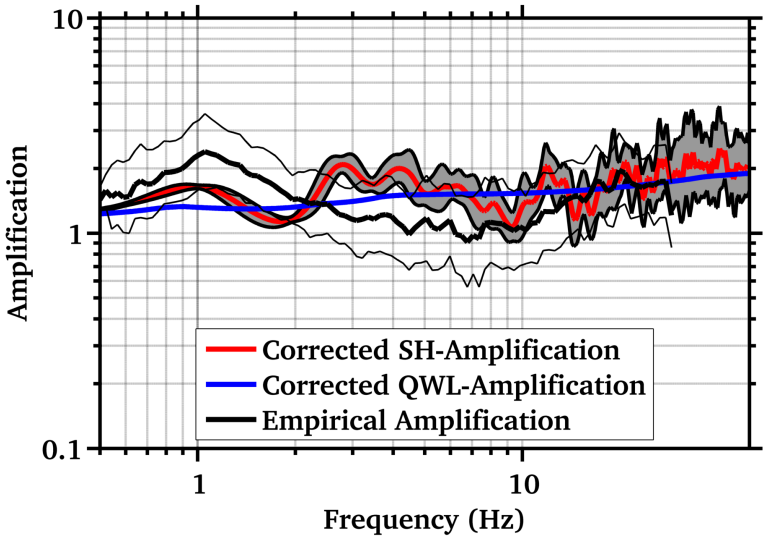

Figure 22 - *Comparison between modeled amplification functions computed using the SH-wave transfer function and the quarter-wavelength formalism with observed empirical amplification from Earthquake spectral fitting (Edwards and Fäh, 2013). All the functions are referenced to the Swiss rock reference model (Poggi et al. 2011).*

12. Engineering soil parameters

The ensemble of all the best inverted velocity profiles is then used to derive average soil parameters like the VsZ (average travel-time S-wave velocity over the depth Z, including Vs30, **Table 1**) and the quarter-wavelength (QWL) average velocities (Joyner et al., 1984) for a range of frequencies between 0.6 and 30Hz (**Figure 23**). The former is a standard parameter for the classification of ground-types in most building codes and in ground motion prediction equations. The latter is a parameter useful for the empirical estimation of the site-response and to assess the sensitivity of the seismic wave-field to the different depths. It has to be noticed that these two parameters are derived separately from all the best S-wave velocity models obtained from the inversion, and the results is finally averaged to improve statistics.

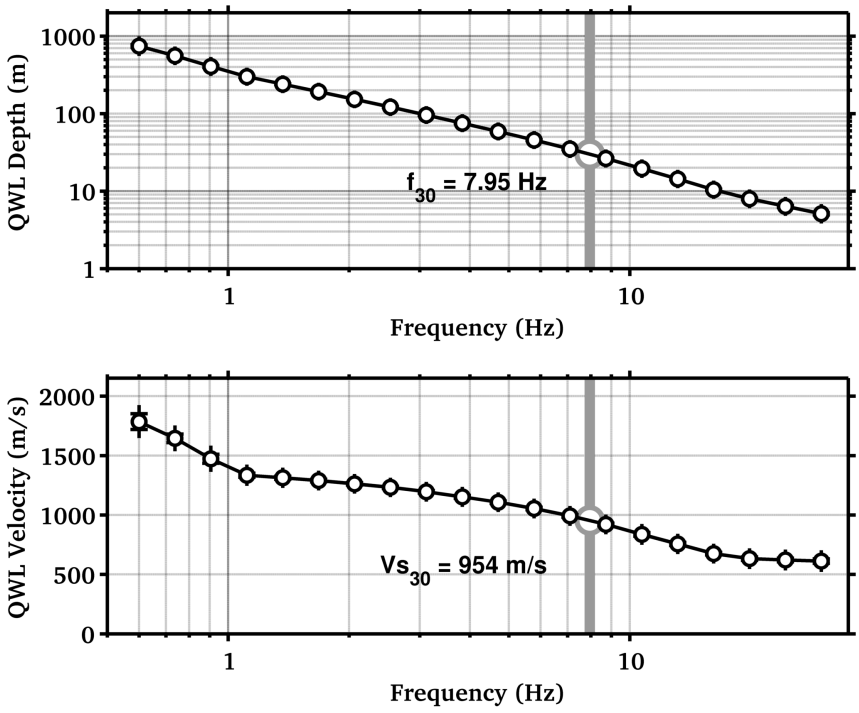

Figure 23 - *Quarter-wavelength representation of the inverted S-wave velocity profiles from the "single mode" model. Top: the depth-frequency dependency. Bottom: the QWL average velocity. The Vs30 value is indicated with its corresponding QWL frequency.*

Averaging depth (m)	Vs-mean (m/s)	St.Dev.
5	611.916	17.02094
10	665.9669	8.102553
15	768.0926	7.986122
20	843.8919	9.470917
25	906.2958	7.852841
30	954.3979	8.363619
40	1024.602	8.108233
50	1074.296	8.152109
75	1151.914	9.642955
100	1202.775	8.382917
150	1260.223	8.431377
200	1294.471	9.926153

Table 1 - *Average travel-time velocities at different depths. Vs30 is highlighted.*

REFERENCES

Capon, J., 1969. High resolution frequency wavenumber spectrum analysis, Proc. IEEE, 57, 1408-1418.

Burjanek, J., G. Stamm, V. Poggi, J.R. Moore, and D. Fäh [2010], "Ambient vibration analysis of an unstable mountain slope", Geophys. J. Int., Vol. 180, pp. 820-828.

Edwards, B., C. Michel, V. Poggi and D. Fäh (2013). Determination of Site Amplification from Regional Seismicity: Application to the Swiss National Seismic Networks. Accepted for publication in Seismological Research Letters.

Edwards, B. and D. Fäh (2013). A Stochastic Ground-Motion Model for Switzerland, Bulletin of the Seismological Society of America, 103 (1), 78-98.

Joyner, W. B., R. E. Warrick and T. E. Fumal (1981). The Effect of Quaternary Alluvium on Strong Ground Motion in the Coyote Lake, California, Earthquake of 1979, Bulletin of the Seismological Society of America, 71, 1333-1349.

Poggi, V., B. Edwards and D. Fäh (2011). Derivation of a Reference Shear-Wave Velocity Model from Empirical Site Amplification, Bulletin of the Seismological Society of America, 101, 258-274.

Poggi, V. and Fäh D., 2010. Estimating Rayleigh wave particle motion from three-component array analysis of ambient vibrations. Geophys. J. Int., 180-1, 251-267.